Chemical Science

ROYAL SOCIETY OF CHEMISTRY

EDGE ARTICLE

View Article Online
View Journal | View Issue

Cite this: *Chem. Sci.*, 2025, **16**, 1995

All publication charges for this article have been paid for by the Royal Society of Chemistry

Received 7th October 2024
Accepted 21st December 2024

DOI: 10.1039/d4sc06771a

rsc.li/chemical-science

Molecular engineering of supramolecular polymer adhesive with confined water and a single crown ether†

Qiangqiang Xu,[a] Paulina Szymoniak,[b] Mohamed Aejaz Kolmangadi,‡[b] Zerui Yang,[a] Shixian Wang,[cd] Yurui Gao,*[cd] Jie Shang,[a] Johannes Hunger,[e] Aitkazy Kaisha,[f] Abdurakhman Aldiyarov,[g] Andreas Schönhals,[*bh] Yan Ge*[a] and Zhenhui Qi[*a]

Here, we report a water-induced supramolecular polymer adhesive formed from confined water and an intrinsically amphiphilic macrocyclic self-assembly in a nanophase-separated structure. The selenium-containing crown ether macrocycle, featuring a strong hydrophilic hydrogen-bond receptor (selenoxide) and a synergistic hydrophobic selenium-substituted crown core, confines water within a segregated, interdigitated architecture. While water molecules typically freeze around 0 °C, the confined water in this supramolecular polymer remains in a liquid-like state down to −80 °C. Previous studies suggested that multiple crown ether units are required to generate confined water; however, in this case, a single unit is sufficient to control the formation and disappearance of confined water, driving supramolecular polymerization. Typically, the DC conductivity of water follows an Arrhenius temperature dependency ($\ln \sigma_{DC} \propto 1/T$). In contrast, this new crown ether unit maintains water in confined states, exhibiting Vogel–Fulcher–Tammann behavior ($\ln \sigma_{DC} \propto 1/(T - T_0)$) at temperatures above the glass transition. Moreover, this water-induced supramolecular polymer demonstrates remarkable adhesion to hydrophilic surfaces, maintaining strong adhesion even at low temperatures. These findings illustrate how a single small macrocycle can control the complex structure and functionality of water in supramolecular systems.

Introduction

Molecular engineering of adhesives plays a pivotal role in industrial applications, including semiconductors,[1] smartphones,[2] aerospace,[3] and medical devices.[4–7] Strong intermolecular interactions and precise molecular structures are essential for achieving accurate viscosity modification, providing greater flexibility in product design and addressing specialized application challenges.[8] Notably, confined water has attracted significant attention for its unique properties and relevance in various scientific and technological fields.[9,10] When confined within nanoscale spaces such as channels,[11–15] pores,[16–18] or between material layers,[19–21] water behaves differently from its bulk form.[22] In adhesives, confined water is crucial in forming strong hydrogen-bond networks, with water molecules exhibiting bonding strengths comparable to ice.[23–26]

Previously, we reported a groundbreaking study in which confined water acted as an essential co-monomer in supramolecular polymerization.[23] Building on our earlier findings, Dong *et al.* extended the study of confined water to a pillararene-crown ether system.[25] In this configuration, ten benzo-21-crown-7-ether units were intricately arranged on the upper and lower rims of pillar[5]arene, highlighting the potential of

[a]*Sino-German Joint Research Lab for Space Biomaterials and Translational Technology, Synergetic Innovation Centre of Biological Optoelectronics and Healthcare Engineering, School of Life Sciences, Northwestern Polytechnical University, Xi'an, Shaanxi 710072, P. R. China. E-mail: qi@nwpu.edu.cn; ge@nwpu.edu.cn*

[b]*Bundesanstalt für Materialforschung und -prüfung (BAM), Unter den Eichen 87, 12205 Berlin, Germany. E-mail: andreas.schoenhals@bam.de*

[c]*Laboratory of Theoretical and Computational Nanoscience, National Centre for Nanoscience and Technology, Chinese Academy of Sciences, Beijing 100190, China. E-mail: gaoyr@nanoctr.cn*

[d]*University of Chinese Academy of Sciences, Beijing 100049, P. R. China*

[e]*Max Planck Institute for Polymer Research Ackermannweg 10, 55128 Mainz, Germany*

[f]*Renewable Energy Laboratory, National Laboratory Astana (NLA), Nazarbayev University, Astana, 010000, Kazakhstan*

[g]*Al-Farabi Kazakh National University, Al-Farabi Av., 71, 050040 Almaty, Kazakhstan*

[h]*Institut für Chemie, Technische Universität Berlin, Straße des 17. Juni 135, 10623 Berlin, Germany*

† Electronic supplementary information (ESI) available: The synthesis and characterization of compounds presented in this work, the experimental details, the simulation details and additional data of tests/simulations. See DOI: https://doi.org/10.1039/d4sc06771a

‡ Physics & Material Science EMEA, Covestro Deutschland AG, 51373 Leverkusen, Germany.

crown ethers with confined water as promising supramolecular adhesive materials.

Driven by curiosity, we sought to understand the functional elements that regulate confined water at the molecular level and identify supramolecular units capable of generating and sustaining confined water. However, the mechanisms behind controlling confined water at the molecular level remain poorly understood, and the development of supramolecular units capable of generating confined water is still limited. Unlocking this understanding could open new pathways in adhesive technology and material science. Macrocycles and host molecules have shown potential in mimicking biological processes such as enzyme catalysis and ion channels.[27–30] However, their role in controlling confined water and mediating non-covalent interactions in adhesive systems remains underexplored.

In this work, we demonstrate that confined water features can now be achieved using a single crown ether macrocycle. Substituting one oxygen atom in the crown ether with selenium imparts unprecedented amphiphilicity to the original **C7** crown ether (Fig. 1a). As a result, this crown ether macrocycle functions like a "Molecular Sheepdog", guiding the formation of confined water.[31] This intriguing behavior stems from the hygroscopic, flexible, and elastic properties of the selenoxide-substituted crown ether, which promotes the confining of water by the macrocycle. Broadband dielectric spectroscopy (BDS), fast scanning calorimetry, thermogravimetric analysis, and vibrational spectroscopy confirm the presence of confined water in the **C7SeO**–water complex, which can also be regarded as a **C7SeO**–water copolymer. Computer simulations further reveal that **C7SeO** molecules tightly confine large clusters of confined water, with selenoxide serving as an excellent hydrogen-bond acceptor. This finding is consistent with previous studies indicating that hydrogen bonding in selenoxide-containing compounds is significantly stronger than in their ether counterparts. Accordingly, this selenoxide-containing crown ether offers a simple model system for studying confined water, including the structural elements and low-temperature functionalities that give rise to its unique properties.

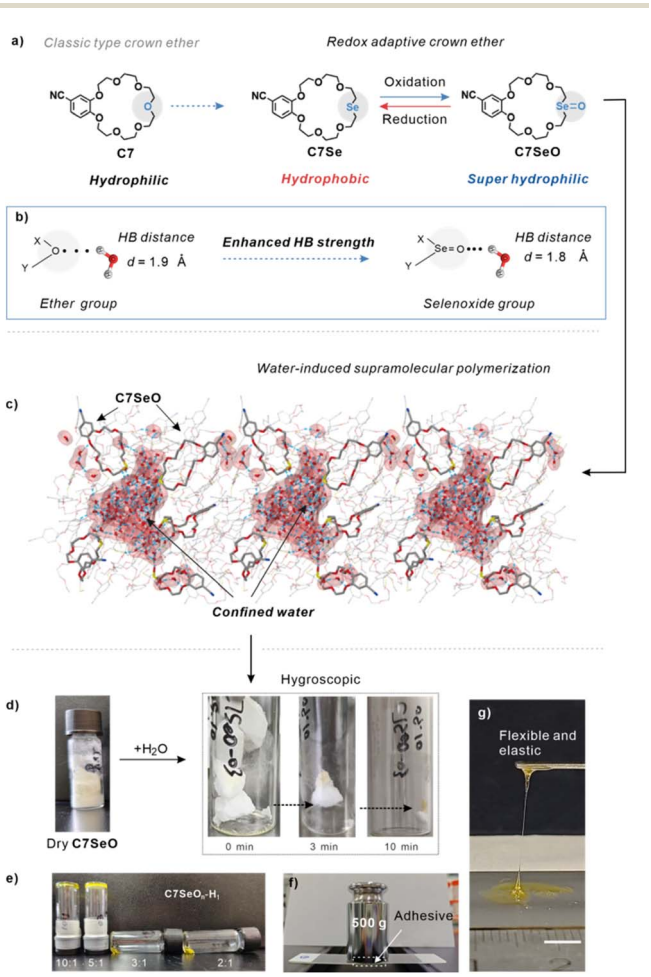

Fig. 1 Properties of selenoxide-modified crown ether macrocycles containing structural water. Through precise structural control, the modified macrocyclic structures acquire structural water components, leading to their incorporation into supramolecular assemblies with high-viscosity adhesive properties, as reported previously.[23,25] (a) Chemical structures of **C7SeO** and its control **C7**. (b) Design principle of enhanced hydrogen bonding behaviour of selenoxide groups compared to ether groups. (c) Illustration of macrocycle-structural water-based supramolecular polymers, where water molecules act as a comonomer for supramolecular polymerization. (d) The dry **C7SeO** sample absorbs water from the ambient humidity (from a white fluffy to yellow sticky solid). (e) Pictures of the **C7SeO** samples featuring varying water content [$C7SeO_n$-H_1 is used to abbreviate samples with **C7SeO** : water (H) ratio of n : 1 (w/w)]. (f) The macroscopic adhesive properties of $C7SeO_{10}$-H_1 materials with a hydrophilic glass surface (with an adhesion area measuring 2.0 × 2.5 cm^2). The material, located within a glass-adhesive-glass sandwich, is marked with a white dotted box. (g) Photograph of the hydrogel filament drawn from the $C7SeO_{10}$-H_1 reservoir. The scale bar is 0.5 cm.

Results

Selenoxide crown ether C7SeO: confined water and supramolecular polymerization

As shown in Fig. 1a, the selenoxide-containing crown ether **C7SeO** (differing by only one atom from **C7**) serves as a suitable model system for assessing structural water and its contributing elements. Based on previous crystal structures and theoretical modeling studies, the hydrogen bond distance of the selenoxide group (1.8 Å) is shorter than that of an ether (–O–) group (1.9 Å).[32,33] Therefore, the selenoxide group is expected to behave as a better hydrogen bond acceptor compared to the ether group (Fig. 1b). We prepared a selenide-substituted crown ether initially, which can be further oxidized into the selenoxide form. The obtained **C7SeO** compound was thoroughly characterized to confirm the desired structure (refer to the detailed description in the ESI, Fig. S1–S5†). The electrostatic potential calculations indicate that the selenoxide region of **C7SeO** exhibits strong hydrogen-bond acceptor properties, while the crown ether moiety remains highly hydrophobic (Fig. S1b†). In contrast, the reduced form of **C7Se** is completely hydrophobic, consistent with our previous findings.[34] Studies have established a direct correlation between the hydrogen bonding strength and hydration.[35] The crown ether **C7** has been reported to exhibit a sharp order-disorder phase transition with a lower

critical solution temperature.[36] Heating an aqueous solution of **C7** results in an entropic breakdown of the hydrogen bonds between the ethylene glycol rings and water molecules, forming a more hydrophobic macrocycle that phase separates from the aqueous solution (Fig. S6†). Under identical conditions, however, the selenoxide-substituted **C7SeO** sample yields a completely transparent solution across the entire temperature range, providing evidence of an enhanced hydrogen bonding in **C7SeO** compared to those of **C7**.

In the dry state, **C7SeO** is a fragile, fluffy solid and has an amorphous structure. However, when exposed to an ambient environment (25 °C, 40% relative humidity), the dry **C7SeO** powder quickly adsorbed water from the ambient humidity (Fig. 1d), resulting in a **C7SeO**–water mixture with easy processability (Fig. 1e) as well as adhesive (Fig. 1f and Scheme S1†), flexible and elastic properties (Fig. 1g). This behaviour closely resembles the characteristics of molecules that possess confined water[23] and is notably distinctive compared to the related control compound **C7** (Fig. S10†), which shows no weight gain or significant decrease in viscosity upon exposure to ambient air. This result evidence that the selenoxide group is responsible for the water-induced supramolecular polymerization of this hydrogen bonding-enhanced crown ether.

Evidence of confined water from BDS and Flash-DSC

BDS investigations were performed to study the states of the water molecules in the **C7SeO$_n$-H$_1$** supramolecular polymers.[23] The molecular mobility of water within the discussed supramolecular system are predominantly controlled by its interactions with the crown ether molecules. Consequently, various states of water, such as bulk-like, confined water, can be discerned and characterized.[23] The real part of the complex conductivity for **C7SeO$_5$-H$_1$** shows the expected frequency dependence typical for semiconducting materials (Fig. S12†).[37] The observed plateau in the data at low frequencies corresponds to the DC conductivity σ_{DC}, which is estimated by fitting the Jonscher equation to the data. The Jonsher equation reads

$$\sigma'(f) = \sigma_{DC}\left(1 + \left(\frac{f}{f_c}\right)^k\right)$$

Here, f_c is a characteristic frequency characterizing the onset of the dispersion. The exponent k varies between 0.5 and 1.0.

As shown in Fig. 2a, for weight ratios of **C7SeO$_n$-H$_1$** for $n \geq 5$, the Arrhenius plots of σ_{DC} over $1/T$ do not reveal any discontinuity around the freezing temperature (0 °C) of bulk-like water. This suggests that up to this weight ratio, the supramolecular polymer contains significant amounts of tightly bonded non-freezable water molecules. In contrast, **C7SeO$_3$-H$_1$** and **C7SeO$_2$-H$_1$** exhibit a discontinuity in the dependence of σ_{DC} *versus* $1/T$ near the freezing temperature of water indicating the presence of substantial amounts of bulk-like water. As shown in Fig. 2b, the cooling curve (empty rhombus) exhibits similar temperature dependence of the dielectric loss than the heating curve (solid rhombus), indicating that the water content remains unchanged throughout the heating process. This observation gives further evidence that the water present in

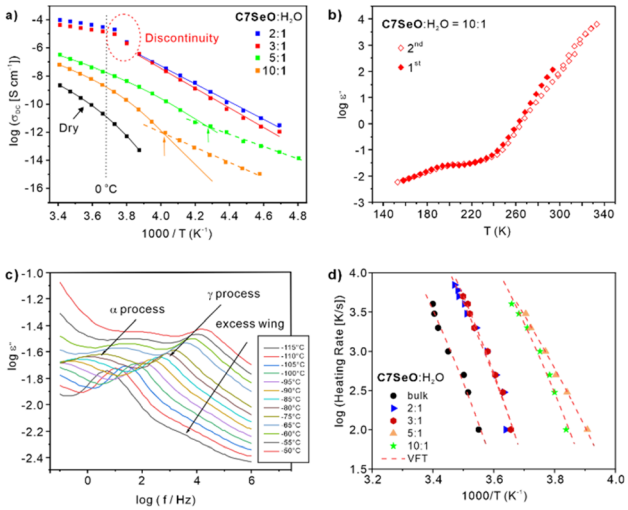

Fig. 2 (a) Dependence of the DC conductivity σ_{DC} *versus* $1/T$ for **C7SeO$_n$-H$_1$** materials with different water contents. (b) Temperature dependence of the dielectric loss (log ε'') at a frequency of 1000 Hz for **C7SeO$_{10}$-H$_1$** for the heating and subsequent cooling cycle. The cooling curve (empty rhombus) shows a behaviour similar to that of the heating curve (solid rhombus). (c) Dielectric loss *versus* frequency for a **C7SeO$_{10}$-H$_1$** adhesive at the indicated temperatures. (d) Heating rate *versus* inverse glass transition temperature estimated by fast scanning calorimetry for **C7SeO$_n$-H$_1$**. Dashed lines are fits of the Vogel–Fulcher–Tammann (VFT) equation to the data.

C7SeO$_{10}$-H$_1$ is confined water which cannot easily change its state during heating.

The dielectric loss spectra of **C7SeO$_{10}$-H$_1$** (Fig. 2c) further reveal distinctive features associated with the presence of confined water, at temperatures from −115 to −50 °C. The spectra resemble that of a homogeneous amorphous polymeric material with a localized γ process at low temperatures and an α relaxation at higher temperature.[37] The emergence of one α process evidences the formation of strong hydrogen bonds between the water molecules and surrounding **C7SeO** molecules, leading to joint cooperative motion of water together with the **C7SeO** molecules.[23,37] Also the frequency position of the γ process shifts to higher frequencies with increasing temperature indicating the formation of a homogeneous structure of water molecules with **C7SeO** (see Fig. S13†). Fig. S14† compares the dielectric loss spectra of **C7SeO$_{10}$-H$_1$** with that of dry **C7SeO**. For both samples, a γ process and the α relaxation are observed. First, the absolute value of the dielectric loss is higher for **C7SeO$_{10}$-H$_1$** compared to **C7SeO**. This is due to the higher dipole moment of the incorporated water molecules. Secondly, for **C7SeO$_{10}$-H$_1$**, the α relaxation shifts to lower frequencies compared to the dry material (Fig. S15†). This shift points to an increased interaction between the water molecules and **C7SeO** due to hydrogen bonds. With the increase of the concentration of water, the intensity of the γ relaxation is approximately constant till the composition of 5 : 1 (Fig. S16†). For higher concentrations of water, the intensity of the γ relaxation increases strongly with the water content. Fig. S16† displays two distinctive regimes in the concentration dependence of the

intensity of the γ relaxation indicating two different states of water in the system. A high-frequency tail, also referred to as excess-wing, is observed,[37] indicating the glass-forming nature of the **C7SeO$_{10}$-H$_1$** supramolecular polymer.

As depicted in Fig. 2a for **C7SeO$_{10}$-H$_1$** and **C7SeO$_5$-H$_1$**, in the temperature region (−30 to −40 °C), the plot of log(σ_{DC}) *versus* inverse of temperature exhibits a pronounced Vogel/Fulcher/Tammann temperature dependence which is characteristic for a glassy behavior of water. In other words, the temperature dependence shows a pronounced "fragile" behavior.[38] Moreover, a distinct crossover phenomenon from the VFT at higher temperatures to an Arrhenius-like behavior at lower ones is observed for **C7SeO$_{10}$-H$_1$** and **C7SeO$_5$-H$_1$**. This crossover takes place approximately at T_g of the system estimated by fast scanning calorimetry (see below) which is a characteristic of confined water, also discussed in the literature.[39] Sometimes this behavior is called strong/fragile transition of confined water. This behavior involves a change in the conduction mechanism. For example, in the case of **C7SeO$_{10}$-H$_1$**, at temperatures above the crossover, the charge transport is coupled with cooperative motions related to the glassy dynamics of the entire system (**C7SeO**–water). Below the crossover temperature, water molecules become trapped in the frozen matrix (**C7SeO** molecules), restricting their mobility, which closely resembles previously reported behaviors of confined water systems. A similar crossover is also observed in **C7SeO$_5$-H$_1$**, which also contains only confined water. For the samples with high water concentration after the freezing transition the temperature dependence of the DC conductivity shows only an Arrhenius or strong behavior which is expected for ice.

The fast differential scanning calorimetry (Flash-DSC) results highlight the thermal behaviour of **C7SeO$_n$-H$_1$** supramolecular polymers, emphasizing the confined water features. Flash-DSC enables heating rates in the range from 0.5 K s^{-1} to 10^4 K s^{-1}. By using these high heating rates, Flash-DSC allows to minimize the evaporation of water from the samples during the measurement.[40] Examples for the measured heat flow curves are given in the ESI (see Fig. S17).† Fig. 2d shows the heating rate *versus* the estimated reciprocal glass transition temperature in the Arrhenius diagram for various **C7SeO$_n$-H$_1$** samples. The experimental data can be described by the Vogel–Fulcher–Tammann (VFT) equation, indicating that all **C7SeO$_n$-H$_1$** are supramolecular glass formers. Notably, a considerable difference in the behaviour is observed between **C7SeO$_{10}$-H$_1$** and **C7SeO$_5$-H$_1$** in comparison to **C7SeO$_3$-H$_1$** and **C7SeO$_2$-H$_1$**, where for the latter the glass transition is observed at higher temperatures. This distinction implies significant differences in the characteristics of confined water features within **C7SeO$_{10}$-H$_1$**/**C7SeO$_5$-H$_1$**, in contrast to **C7SeO$_3$-H$_1$**/**C7SeO$_2$-H$_1$**.[41] For the samples with a high concentration of water (**C7SeO$_3$-H$_1$** and **C7SeO$_2$-H$_1$**) the data collapse approximately into one chart. This is different for the samples with a low concentration of water where the data are shifted to essentially lower temperatures. This becomes clearer in Fig. S18† where the glass transition temperature T_g at a heating rate of 100 K s^{-1} is plotted *versus* the concentration of water. T_g decreases from the bulk state with increases water concentration till **C7SeO$_5$-H$_1$** continuously. For higher water concentration than 5 : 1 an abrupt change in that dependence takes place indicating a radical change in the structure of water in the system (see also Table S2†). These findings suggest that for **C7SeO$_3$-H$_1$**/**C7SeO$_2$-H$_1$**, besides the tightly bonded water, also bulk-like water molecules are present, whereas for **C7SeO$_{10}$-H$_1$**/**C7SeO$_5$-H$_1$** only the former is present. Moreover, the data for **C7SeO$_{10}$-H$_1$** are shifted to higher temperatures compared to **C7SeO$_5$-H$_1$** due to an increased plastification. In that sense, the Flash-DSC results provide further evidence of the presence of two distinctly different states of water within the **C7SeO$_n$-H$_1$** system. We found that **C7SeO** with free water (*e.g.*, **C7SeO$_2$-H$_1$**, **C7SeO$_3$-H$_1$**) has T_g values near 0 °C, which is close to the icing point. In contrast, confined water with **C7SeO** exhibits much lower T_g values, implying that the water retains higher mobility at low temperatures, as corroborated by the dielectric results shown in Fig. 2c.

The confined water dehydration was comprehensively evaluated using thermogravimetric analysis (TGA) of **C7SeO$_n$-H$_1$** (Fig. S19†). The resulting multi-step TG curve of **C7SeO$_{10}$-H$_1$** exhibited two water loss steps (Fig. S20†).[42] The initial step is distinguished by a water content (n_w) of 0.28H$_2$O per crown ether unit, and the second step manifests an n_w of 0.86H$_2$O per crown ether unit, characterized by extrapolated onset and end temperatures of ∼60 °C and 180 °C, respectively (see detail calculation process in ESI†). Similarly, the other **C7SeO$_n$-H$_1$** variants (n = 5, 3, 2) exhibit a comparable pattern, albeit with variations in the specificities of bonded water molecules (Fig. S20 and Table S3†).

Generally, the strength of hydrogen bonds correlates with vibrational frequency: more strongly bonded water molecules exhibit lower OH stretching frequencies. Thus, one could learn about H-bonding strength in the confined water containing

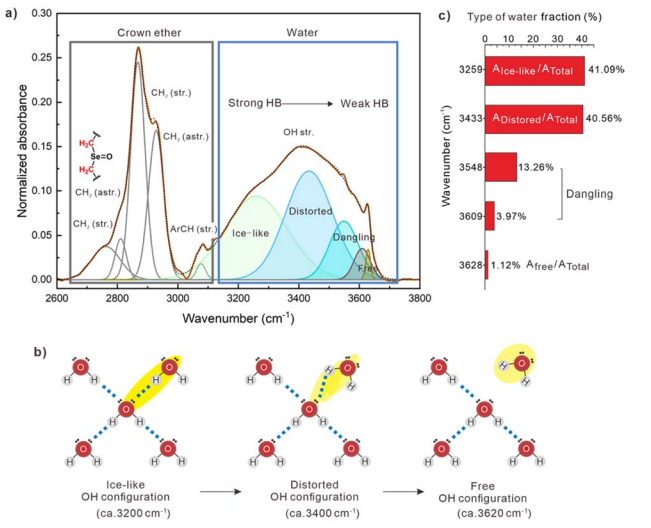

Fig. 3 (a) Illustrative fitting of FTIR spectra within the 2600–3800 cm^{-1} range for **C7SeO$_{10}$-H$_1$** at 25 °C. (b) Schematic depiction of three distinct types of OH configurations in the water network. (c) Percentage distribution of ice-like, distorted, and free OH stretching components derived from the fitting of FTIR spectra for **C7SeO$_{10}$-H$_1$**.

samples and compare it to that of bulk water. Fourier-transform infrared (FTIR) spectroscopy was employed to examine the static state of the hydrogen bond network of water confined within **C7SeO**–H_2O supramolecular polymers. We focused our attention on **C7SeO**$_{10}$-H_1 in the following experiments [the FTIR results of **C7SeO**$_n$-H_1 (n = 5, 3, 2, 1) materials are shown in ESI, Fig. S24†]. Within the spectral range from 2600 to 3800 cm^{-1}, valuable information regarding both the water network's structure through the OH-stretching band and the conformation of the crown ether ring through the CH_2 symmetric and asymmetric stretching vibrations can be derived (Fig. 3a). To capture variations in the H-bonded structure of water, we employed a model for the OH stretching band involving five Gaussian functions.[43] These functions mainly represent ice-like, distorted, and free configurations within the water network, exhibiting a tendency toward higher frequencies (Fig. 3b). The ice-like configuration, at a lower frequency (approximately 3200 cm^{-1}), arises from the ordered H-bond contribution, where water molecules are tetrahedrally coordinated. The distorted configuration refers to the "closed" water structure, where H-bonds are partially distorted. The free configuration results from OH groups weakly stabilized by H-bond interactions (around 3600 cm^{-1}). All these OH oscillator configurations exist in a dynamic equilibrium with each other and are transiently generated during the H-bond reorganization of the water network. We found that the over 98% fractions of water in the **C7SeO**$_{10}$-H_1 supramolecular polymer is H-bonded [*e.g.* the H-bonded ratio of the ice-like component ($A_{\text{ice-like}}/A_{\text{tot}}$, peak around the wavelength 3259 cm^{-1}) reaches to 41.09% (Fig. 3c)]. As anticipated, the fraction of free water is remarkably low, accounting for only 1.12%, which is consistent with the macroscopic and BDS characterization results.[44–46] This may explain why **C7SeO**$_{10}$-H_1 exhibits adhesion (Fig. 1f) to a glass surface, as its OH groups are mostly strongly intermolecular H-bonded.

Molecular dynamics simulations for confined water

To investigate the form of water in the **C7SeO** and H_2O mixtures, atomistic molecular dynamics (MD) simulations were performed for the **C7SeO**$_{10}$-H_1 system. The system composed of 400 **C7SeO** molecules and 1000 water molecules, was maintained in the constant-pressure and constant-temperature (*NPT*) ensemble for 400 ns at 240 and 270 K, respectively. Fig. 4a demonstrates the equilibrium structure of the system at 240 K, revealing a relatively large water cluster/ball approximately 2–4 nm in size (Fig. 4bI and II), containing ~800 water molecules. The **C7SeO** molecules at the interface of the water cluster were oriented with selenoxide groups pointing inward, forming strong hydrogen bonds with water molecules. This behavior is due to the amphiphilic nature of **C7SeO**, where the selenoxide (SeO) head group forms strong hydrogen bonds with water molecules, while the crown ether core creates a hydrophobic domain, confining water within the aggregated state of **C7SeO**.

Moreover, the interface of the confined water was always rough with bulges, increasing the contact area and the total interfacial hydrogen-bond interactions, due to the stronger

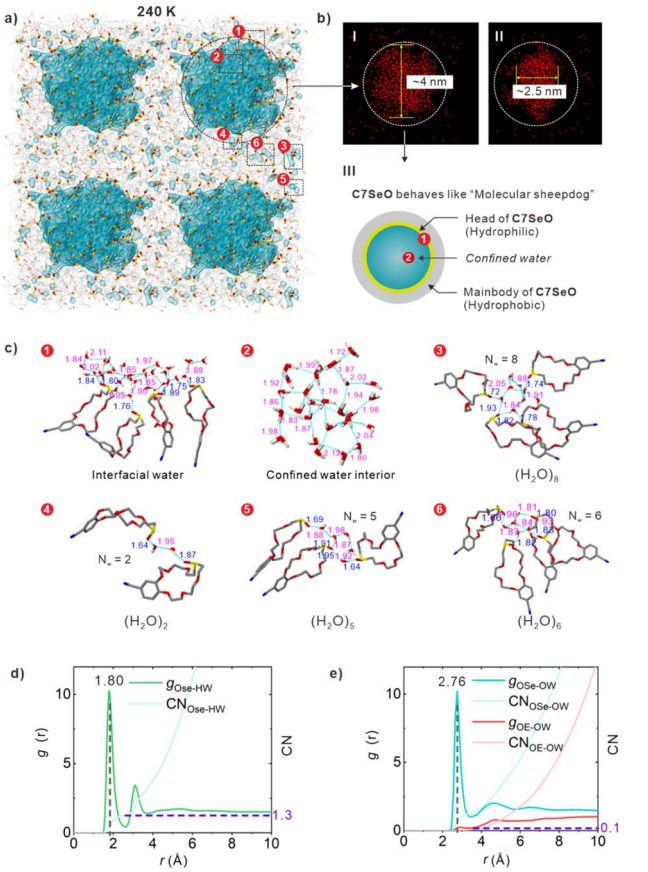

Fig. 4 (a) Equilibrium snapshot of the **C7SeO**$_{10}$-H_1 system from MD simulations at 240 K, exhibiting a large water ball and some dispersive water molecules or clusters among the **C7SeO** molecules. Water ball/clusters are coloured by light blue. **C7SeO** molecules are presented by grey line, and Se and O atoms in selenoxide groups are specially shown in yellow and red sticks, respectively. (b) Images showing (I and II) the size of the simulated water ball in **C7SeO**$_{10}$-H_1 and (III) a diagram of a confined water ball architecture, illustrating the water core and the interfacial water layer.[31] (c) Structure of (①) the interface and (②) the interior of the water ball, and (③–⑥) structure of example dispersive water clusters forming hydrogen bonds with **C7SeO** molecules. H, C and N atoms in **C7SeO** molecules are shown in white, grey and blue sticks. Hydrogen bonds are indicated by light blue dashed lines. N_w represents the number of water molecules in the cluster. (d) Radial distribution functions (RDFs) of the O atoms in selenoxide groups (denoted by OSe) and H atoms in water molecules ($g_{\text{OSe–HW}}$), and the corresponding coordination numbers ($\text{CN}_{\text{OSe–HW}}$). $\text{CN}_{\text{OSe–HW}}$ amounts to approximately 1.3 at the maximum of the first coordination distance, indicating that each selenoxide group, on average, forms 1.3 hydrogen bonds with water molecules. (e) RDFs of the O atoms in selenoxide groups and O atoms in water molecules ($g_{\text{OSe–OW}}$), and O atoms in ether group (denoted by OE) and O atoms in water molecules ($g_{\text{OE–OW}}$), respectively, and the corresponding $\text{CN}_{\text{OSe–OW}}$ and $\text{CN}_{\text{OE–OW}}$. Notably, **C7SeO** molecules shown in the figures include only those forming hydrogen bonds with water molecules.

HOH···OSe hydrogen bond. We found that the first adsorbed water molecule generally occurred through the short H-bonds to the selenoxide group (averaging 1.8 Å) similar to other water-adsorption systems.[47] Importantly, significant smaller water clusters, ranging from 56 water monomers, 10 water dimers, 3 water trimers, 1 pentamer, 1 water hexamer to 1

octamer, were also observed (Fig. 4c and S25a†) dispersed among the **C7SeO** molecules. Interestingly, a single water molecule could have two hydrogen bond interactions with two adjacent selenoxide groups. A water dimer formed one hydrogen bond between the two water molecules within the dimer while formed two stronger hydrogen bond interactions with two adjacent selenoxide groups. Larger water clusters created hydrogen bond networks among water molecules, and form additional hydrogen bond with adjacent selenoxide groups.

Notably, two kinds of hydrogen bonds were involved here, the water–water and water–OSe hydrogen bonds. Compared to the former, the latter bond has a shorter length of ~1.80 Å, corresponding to the position of the first peak of g_{OSe-HW} in Fig. 4d. Hence, the distance between the nearest O (in selenoxide group) and O (in water molecule) atoms was 2.76 Å (Fig. 4e), coincidentally with the nearest O–O distance of ice in the form of Ih. The hydrogen bond energy (E_{HB}) between the selenoxide group and water, with the O atom in a selenoxide group acting as a stronger hydrogen bond acceptor, was estimated to be −0.313 eV (Fig. S28†), approximately 0.1 eV lower than that of the water dimer (−0.215 eV), indicating a stronger interaction. In contrast, this value is close to the binding strength of hydrogen bonds in bulk ice Ih, possibly explaining the observed ice-like vibration peak in the FTIR spectra. In the total system, each selenoxide group could averagely form 1.3 hydrogen bonds with water molecules, while the number of water molecules around ether groups and cyano groups was only 0.1 and 0.2, respectively, which was negligible (Fig. 4e and S25b†). The stronger OSe–water hydrogen bond interactions combined with the water clusters or even water balls, play a key role in the "sticky" nature of the liquid system. Additionally, consistent results were observed for the **C7SeO$_{10}$-H$_1$** system at 270 K as shown in Fig. S26.†

Low-temperature adhesion properties

One unique feature of above discussed confined water is its antifreeze property; this means that the herein water typically exhibits a significantly lower freezing point than bulk water or is even unfreezable.[23,25,48–50] Tough adhesion at low temperatures is an excellent advantage for practical adhesives applications.[23,25,51,52] Therefore, the material considered in this study is captivating from a fundamental perspective due to the distinctive role of water as an essential comonomer for low-temperature supramolecular polymer adhesive. **C7SeO$_{10}$-H$_1$** supramolecular polymer probably has strong adhesion abilities at low temperatures. Two stainless steel plates stored at different low temperatures were firmly adhered together by **C7SeO$_{10}$-H$_1$**, as can be seen in Fig. 5a. Moreover, robust adhesion of **C7SeO$_{10}$-H$_1$** was observed when the testing temperature rapidly decreased (Fig. 5b and c). At −10 °C, the **C7SeO$_{10}$-H$_1$** adhesive successfully supported a load of 1 kg. Further weight tolerances were demonstrated in a low-temperature range from −20 to −40 °C. The increased resistance to low temperatures in the **C7SeO**–water copolymer is attributed to the enhanced hydrogen bonding force. In lap shear tests, **C7SeO$_{10}$-H$_1$** exhibited an adhesion strength of 2.36 MPa at −40 °C, significantly surpassing the adhesion strengths of samples with **C7** analogue, which was only 0.75 MPa, comparable to that of pure water (0.36 MPa). Notably, this value is comparable to those reported for polymer adhesives and entities having multiple crown ethers (Table S4†). This highlights the significant role of the selenoxide group in **C7SeO** in promoting adhesive performance at low temperatures. While correlating the low-temperature adhesive performance with T_g (see Table S2 and Fig. S18†), our experiments conducted at −40 °C, which is well below the T_g given in Fig. 2d and Table S2,† demonstrating how T_g influences adhesion. This suggests that adhesive properties are enhanced in the glassy state. The flexibility of **C7SeO$_{10}$-H$_1$** was maintained down to −80 °C, as no cracks were observed for **C7SeO$_{10}$-H$_1$** at this temperature (Fig. S28†). In sharp contrast, high-water-content **C7SeO$_n$-H$_1$** samples became turbid solids at low temperatures. These remarkable results emphasize the significance of confined water-composite supramolecular polymers. In these bulk samples, water exhibited an enhanced antifreezing capability compared to that of water as a sole solvent in conventional supramolecular polymers.

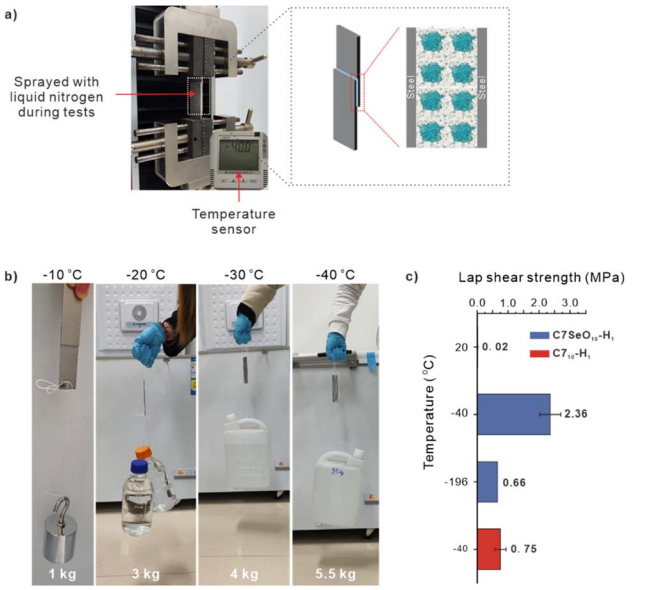

Fig. 5 Application of **C7SeO$_{10}$-H$_1$** materials as adhesive materials at extremely low temperatures. (a) Digital image of lap shear tests performed at −40 °C. Cartoon representation of the adhesion procedure. (b) Macroscopic adhesive behaviour of **C7SeO$_{10}$-H$_1$** materials on a 304 stainless steel surface at various low temperatures. Water was used in these pictures. (c) Lap shear strengths of **C7SeO$_{10}$-H$_1$** and its control **C7$_{10}$-H$_1$**.

Conclusions

In summary, we have demonstrated a rational design of a promising platform for creating confined water in a single crown ether macrocycle. Our research provides a comprehensive understanding of how a single macrocyclic unit can govern the behaviour of confined water, paving the way for further

exploration of confined water in supramolecular systems and their potential applications. The introduction of selenoxide, a stronger hydrogen-bond acceptor, leads to high viscosity and hygroscopic behaviours that distinguish our system from traditional confined water setups. Unlike classical confined water systems, which often rely on complex structures, our advantage lies in generating confined water within a well-defined molecular architecture. This not only significantly enhances our understanding and control over the molecular factors responsible for confined water generation, but also expands the possibilities for designing materials based on confined water. This study provides an in-depth understanding of these molecular factors, emphasizing that the presence of selenoxide is a key advantage. Given the scarcity of supramolecular building blocks containing confined water, the systematic investigation of water behaviour within the confined water-composited supramolecular polymer **C7SeO$_{10}$-H$_1$** opens new pathways for potential applications in adhesives and engineering, while deepening our comprehension of the fundamental principles underlying confined water in materials science.

Data availability

The synthesis and characterization of compounds presented in this work, the experimental details, the simulation details and additional data of tests/simulations are described in the ESI.†

Author contributions

All authors have approved the final version of the manuscript. Q. X., Y. G., and Z. Q. designed and directed the study. P. S., M. A. K. and A. S. performed the BDS and Flash-DSC measurements. Z. Y. and J. S. helped with the synthesis and characterization. S. W. and Y. G. performed the molecular dynamics simulations. J. H. helped with FTIR. Q. X., P. S., A. S. and Z. Q. wrote the manuscript. All the authors commented on the paper.

Conflicts of interest

The authors declare no competing financial interest.

Note added after first publication

This version replaces the manuscript published on 23rd December 2024 which omitted one of the authors from the author list. The RSC apologises for any confusion.

Acknowledgements

We gratefully acknowledge the financial support from the National Natural Science Foundation of China (22071196, 22007078, 21901210, 22273014 and 22471220), National Key Research and Development Program of China (Grant No. 2022YFA1203200), Higher Education Research Fund of NPU (CJGZMS202202), National Innovation Training Program for College Students (202210699005), and the Fundamental Research Funds for the Central Universities. We express our gratitude to Prof. Dong Shengyi for assisting with the low-temperature adhesion measurements. We thank the Analytical & Testing Center of NPU for the characterization of materials.

Notes and references

1 N. Li, Y. Li, Z. Cheng, Y. Liu, Y. Dai, S. Kang, S. Li, N. Shan, S. Wai, A. Ziaja, Y. Wang, J. Strzalka, W. Liu, C. Zhang, X. Gu, J. A. Hubbell, B. Tian and S. Wang, Bioadhesive polymer semiconductors and transistors for intimate biointerfaces, *Science*, 2023, **381**, 686–693.

2 Y. Kwon, S. Lee, J. Kim, J. Jun, W. Jeon, Y. Park, H.-J. Kim, J. Gierschner, J. Lee, Y. Kim and M. S. Kwon, Ultraviolet light blocking optically clear adhesives for foldable displays via highly efficient visible-light curing, *Nat. Commun.*, 2024, **15**, 2829.

3 X. Xie, Y. Jiang, X. Yao, J. Zhang, Z. Zhang, T. Huang, R. Li, Y. Chen, S.-L. Li and Y.-Q. Lan, A solvent-free processed low-temperature tolerant adhesive, *Nat. Commun.*, 2024, **15**, 5017.

4 K. R. Jinkins, S. Li, H. Arafa, H. Jeong, Y. J. Lee, C. Wu, E. Campisi, X. Ni, D. Cho, Y. Huang and J. A. Rogers, Thermally switchable, crystallizable oil and silicone composite adhesives for skin-interfaced wearable devices, *Sci. Adv.*, 2022, **8**, eabo0537.

5 N. D. Blelloch, H. J. Yarbrough and K. A. Mirica, Stimuli-responsive temporary adhesives: enabling debonding on demand through strategic molecular design, *Chem. Sci.*, 2021, **12**, 15183–15205.

6 Y. Fang, L. Meng, A. Prominski, E. N. Schaumann, M. Seebald and B. Tian, Recent advances in bioelectronics chemistry, *Chem. Soc. Rev.*, 2020, **49**, 7978–8035.

7 K. G. Stakem, F. J. Leslie and G. L. Gregory, Polymer design for solid-state batteries and wearable electronics, *Chem. Sci.*, 2024, **15**, 10281–10307.

8 K. Zhao, Y. Liu, Y. Ren, B. Li, J. Li, F. Wang, C. Ma, F. Ye, J. Sun, H. Zhang and K. Liu, Molecular Engineered Crown-Ether-Protein with Strong Adhesion over a Wide Temperature Range from −196 to 200 °C, *Angew. Chem., Int. Ed.*, 2022, **61**, e202207425.

9 H. G. Park and Y. Jung, Carbon nanofluidics of rapid water transport for energy applications, *Chem. Soc. Rev.*, 2014, **43**, 565–576.

10 L. Tavagnacco, M. Zanatta, E. Buratti, M. Bertoldo, E. Chiessi, M. Appel, F. Natali, A. Orecchini and E. Zaccarelli, Water slowing down drives the occurrence of the low temperature dynamical transition in microgels, *Chem. Sci.*, 2024, **15**, 9249–9257.

11 G. Hummer, J. C. Rasaiah and J. P. Noworyta, Water conduction through the hydrophobic channel of a carbon nanotube, *Nature*, 2001, **414**, 188–190.

12 T. Ohba, Size-Dependent Water Structures in Carbon Nanotubes, *Angew. Chem., Int. Ed.*, 2014, **53**, 8032–8036.

13 H. Fenniri, G. A. Tikhomirov, D. H. Brouwer, S. Bouatra, M. El Bakkari, Z. Yan, J.-Y. Cho and T. Yamazaki, High Field Solid-State NMR Spectroscopy Investigation of 15N-

Labeled Rosette Nanotubes: Hydrogen Bond Network and Channel-Bound Water, *J. Am. Chem. Soc.*, 2016, **138**, 6115–6118.

14 B. P. Gorshunov, V. I. Torgashev, E. S. Zhukova, V. G. Thomas, M. A. Belyanchikov, C. Kadlec, F. Kadlec, M. Savinov, T. Ostapchuk, J. Petzelt, J. Prokleška, P. V. Tomas, E. V. Pestrjakov, D. A. Fursenko, G. S. Shakurov, A. S. Prokhorov, V. S. Gorelik, L. S. Kadyrov, V. V. Uskov, R. K. Kremer and M. Dressel, Incipient ferroelectricity of water molecules confined to nano-channels of beryl, *Nat. Commun.*, 2016, **7**, 12842.

15 Y. Ishii, N. Matubayasi, G. Watanabe, T. Kato and H. Washizu, Molecular insights on confined water in the nanochannels of self-assembled ionic liquid crystal, *Sci. Adv.*, 2021, **7**, eabf0669.

16 R. Musat, J. P. Renault, M. Candelaresi, D. J. Palmer, S. Le Caër, R. Righini and S. Pommeret, Finite Size Effects on Hydrogen Bonds in Confined Water, *Angew. Chem., Int. Ed.*, 2008, **47**, 8033–8035.

17 J. B. Mietner, F. J. Brieler, Y. J. Lee and M. Fröba, Properties of Water Confined in Periodic Mesoporous Organosilicas: Nanoimprinting the Local Structure, *Angew. Chem., Int. Ed.*, 2017, **56**, 12348–12351.

18 J. S. Bates, B. C. Bukowski, J. Greeley and R. Gounder, Structure and solvation of confined water and water–ethanol clusters within microporous Brønsted acids and their effects on ethanol dehydration catalysis, *Chem. Sci.*, 2020, **11**, 7102–7122.

19 G. Cicero, J. C. Grossman, E. Schwegler, F. Gygi and G. Galli, Water Confined in Nanotubes and between Graphene Sheets: A First Principle Study, *J. Am. Chem. Soc.*, 2008, **130**, 1871–1878.

20 H. Yoshida, V. Kaiser, B. Rotenberg and L. Bocquet, Dripplons as localized and superfast ripples of water confined between graphene sheets, *Nat. Commun.*, 2018, **9**, 1496.

21 D. Muñoz-Santiburcio and D. Marx, Chemistry in nanoconfined water, *Chem. Sci.*, 2017, **8**, 3444–3452.

22 T. Dufils, C. Schran, J. Chen, A. K. Geim, L. Fumagalli and A. Michaelides, Origin of dielectric polarization suppression in confined water from first principles, *Chem. Sci.*, 2024, **15**, 516–527.

23 S. Dong, J. Leng, Y. Feng, M. Liu, C. J. Stackhouse, A. Schönhals, L. Chiappisi, L. Gao, W. Chen, J. Shang, L. Jin, Z. Qi and C. A. Schalley, Structural water as an essential comonomer in supramolecular polymerization, *Sci. Adv.*, 2017, **3**, eaao0900.

24 Q. Zhang, T. Li, A. Duan, S. Dong, W. Zhao and P. J. Stang, Formation of a Supramolecular Polymeric Adhesive via Water–Participant Hydrogen Bond Formation, *J. Am. Chem. Soc.*, 2019, **141**, 8058–8063.

25 X. Li, J. Lai, Y. Deng, J. Song, G. Zhao and S. Dong, Supramolecular Adhesion at Extremely Low Temperatures: A Combined Experimental and Theoretical Investigation, *J. Am. Chem. Soc.*, 2020, **142**, 21522–21529.

26 Z. Qi, Y. Qin, J. Wang, M. Zhao, Z. Yu, Q. Xu, H. Nie, Q. Yan and Y. Ge, The aqueous supramolecular chemistry of crown ethers, *Front. Chem.*, 2023, **11**, 1119240.

27 Z. Dong, Q. Luo and J. Liu, Artificial enzymes based on supramolecular scaffolds, *Chem. Soc. Rev.*, 2012, **41**, 7890–7908.

28 T. Keijer, T. Bouwens, J. Hessels and J. N. H. Reek, Supramolecular strategies in artificial photosynthesis, *Chem. Sci.*, 2021, **12**, 50–70.

29 L. He, T. Zhang, C. Zhu, T. Yan and J. Liu, Crown Ether-Based Ion Transporters in Bilayer Membranes, *Chem.–Eur. J.*, 2023, **29**, e202300044.

30 L. E. Bickerton, T. G. Johnson, A. Kerckhoffs and M. J. Langton, Supramolecular chemistry in lipid bilayer membranes, *Chem. Sci.*, 2021, **12**, 11252–11274.

31 M. D. Fayer and N. E. Levinger, Analysis of Water in Confined Geometries and at Interfaces, *Annu. Rev. Anal. Chem.*, 2010, **3**, 89–107.

32 E. Renault and J.-Y. Le Questel, Selenoxides Are Better Hydrogen-Bond Acceptors than Sulfoxides: a Crystallographic Database and Theoretical Investigation, *J. Phys. Chem. A*, 2004, **108**, 7232–7240.

33 J. P. M. Lommerse, S. L. Price and R. Taylor, Hydrogen bonding of carbonyl, ether, and ester oxygen atoms with alkanol hydroxyl groups, *J. Comput. Chem.*, 1997, **18**, 757–774.

34 L. Jin, B. Li, Z. Cui, J. Shang, Y. Wang, C. Shao, T. Pan, Y. Ge and Z. Qi, Selenium Substitution-Induced Hydration Changes of Crown Ethers As Tools for Probing Water Interactions with Supramolecular Macrocycles in Aqueous Solutions, *J. Phys. Chem. B*, 2019, **123**, 9692–9698.

35 J. C. Foster, I. Akar, M. C. Grocott, A. K. Pearce, R. T. Mathers and R. K. O'Reilly, 100th Anniversary of Macromolecular Science Viewpoint: The Role of Hydrophobicity in Polymer Phenomena, *ACS Macro Lett.*, 2020, **9**, 1700–1707.

36 S. Dong, L. Wang, J. Wu, L. Jin, Y. Ge, Z. Qi and C. Wu, Thermosensitive Phase Behavior of Benzo-21-crown-7 and Its Derivatives, *Langmuir*, 2017, **33**, 13861–13866.

37 F. Kremer and A. Schönhals, *Broadband Dielectric Spectroscopy*, Springer Berlin, Heidelberg, 2003.

38 R. Bergman and J. Swenson, Dynamics of supercooled water in confined geometry, *Nature*, 2000, **403**, 283–286.

39 S. Cerveny, F. Mallamace, J. Swenson, M. Vogel and L. Xu, Confined Water as Model of Supercooled Water, *Chem. Rev.*, 2016, **116**, 7608–7625.

40 M. Kobayashi and H. Tanaka, The reversibility and first-order nature of liquid–liquid transition in a molecular liquid, *Nat. Commun.*, 2016, **7**, 13438.

41 Z. A. Piskulich, O. O. Mesele and W. H. Thompson, Activation Energies and Beyond, *J. Phys. Chem. A*, 2019, **123**, 7185–7194.

42 C. G. Tang, M. N. Syafiqah, Q.-M. Koh, M. C.-Y. Ang, K.-K. Choo, M.-M. Sun, M. Callsen, Y.-P. Feng, L.-L. Chua, R.-Q. Png and P. K. H. Ho, Water binding and hygroscopicity in π-conjugated polyelectrolytes, *Nat. Commun.*, 2023, **14**, 3978.

43 Y. Yao, S. Catalini, B. Kutus, J. Hunger, P. Foggi and R. Mezzenga, Probing Water State during Lipidic Mesophases Phase Transitions, *Angew. Chem., Int. Ed.*, 2021, **60**, 25274–25280.

44 M. Lounasvuori, Y. Sun, T. S. Mathis, L. Puskar, U. Schade, D.-E. Jiang, Y. Gogotsi and T. Petit, Vibrational signature of hydrated protons confined in MXene interlayers, *Nat. Commun.*, 2023, **14**, 1322.

45 Y. Ikemoto, Y. Harada, M. Tanaka, S.-n. Nishimura, D. Murakami, N. Kurahashi, T. Moriwaki, K. Yamazoe, H. Washizu, Y. Ishii and H. Torii, Infrared Spectra and Hydrogen-Bond Configurations of Water Molecules at the Interface of Water-Insoluble Polymers under Humidified Conditions, *J. Phys. Chem. B*, 2022, **126**, 4143–4151.

46 P. N. Perera, K. R. Fega, C. Lawrence, E. J. Sundstrom, J. Tomlinson-Phillips and D. Ben-Amotz, Observation of water dangling OH bonds around dissolved nonpolar groups, *Proc. Acad. Nat. Sci.*, 2009, **106**, 12230–12234.

47 N. Hanikel, X. Pei, S. Chheda, H. Lyu, W. Jeong, J. Sauer, L. Gagliardi and O. M. Yaghi, Evolution of water structures in metal-organic frameworks for improved atmospheric water harvesting, *Science*, 2021, **374**, 454–459.

48 T. Sun, F.-H. Lin, R. L. Campbell, J. S. Allingham and P. L. Davies, An Antifreeze Protein Folds with an Interior Network of More Than 400 Semi-Clathrate Waters, *Science*, 2014, **343**, 795–798.

49 Y.-C. Liou, A. Tocilj, P. L. Davies and Z. Jia, Mimicry of ice structure by surface hydroxyls and water of a β-helix antifreeze protein, *Nature*, 2000, **406**, 322–324.

50 Z. He, C. Wu, M. Hua, S. Wu, D. Wu, X. Zhu, J. Wang and X. He, Bioinspired Multifunctional Anti-icing Hydrogel, *Matter*, 2020, **2**, 723–734.

51 H. Xu, X. Jiang, X. Han, H. Cai and F. Gao, Cooking inspired tough, adhesive, and low-temperature tolerant gluten-based organohydrogels for high performance strain sensors, *J. Mater. Chem. A*, 2021, **9**, 25104–25113.

52 S. Luo, N. Wang, Y. Pan, B. Zheng, F. Li and S. Dong, Supramolecular/Dynamic Covalent Design of High-Performance Pressure-Sensitive Adhesive from Natural Low-Molecular-Weight Compounds, *Small*, 2024, **20**, 2310839.